Effect of nitrogen incorporation in $La_{2/3}Ca_{1/3}MnO_3$ manganite

2002 J. Phys.: Condens. Matter 14 181

(http://iopscience.iop.org/0953-8984/14/2/306)

INSTITUTE OF PHYSICS PUBLISHING JOURNAL OF PHYSICS: CONDENSED MATTER

J. Phys.: Condens. Matter **14** (2002) 181–191 PII: S0953-8984(02)27039-3

Effect of nitrogen incorporation in $La_{2/3}Ca_{1/3}MnO_3$ manganite

Yongquan Guo, Sujoy Roy and Naushad Ali[1]

Department of Physics, Southern Illinois University, Carbondale, IL 62901-4401, USA

E-mail: nali@physics.siu.edu

Received 20 July 2001, in final form 7 November 2001
Published 13 December 2001
Online at stacks.iop.org/JPhysCM/14/181

Abstract

We have studied the crystal structure, the magnetic and electron transport properties and the magnetoresistance effect of nitrogenation of $La_{2/3}Ca_{1/3}MnO_3$ by x-ray powder diffraction, magnetic measurement and standard four-probe resistance–temperature measurement. Nitrogenation results in an increase in the lattice parameter and unit cell volume, and induces the formation of a superlattice. The N atom prefers to occupy the $4c$ crystal position in the superlattice structure. Nitrogenation weakens the ferromagnetic ordering and results in the decrease of Curie temperature and the saturation magnetic moment but increases the electrical resistivity significantly. The electrical resistivity exhibits a metal–insulator (MI) transition, but the MI transition temperature decreases after nitrogenation. The behaviour of the electrical resistivity follows the equation $\rho = \rho_0(1 - aT + bT^2 + cT^4)$ in the metal regime. However, it follows the formula $\rho = \rho_0 \exp(E/k_B T)$ in the insulator regime. The magnetoresistance ratio measurement shows an increase of 15% after nitrogenation.

1. Introduction

In recent years there has been increasing interest in the alkaline-earth metal doped manganite perovskites $R_{1-x}A_xMnO_3$(R = La, Pr, Nd, Sm, Bi; A = Ca, Sr, Ba, Pb) due to their excellent electron transport, magnetic and structural properties [1–3]. Most of these compounds exhibit the metal–insulator (MI) and paramagnetic–ferromagnetic transitions as well as a colossal magnetoresistance (CMR) effect. The double exchange theory, which was first proposed by Zener [4], is used to explain these phenomena. However, many experimental results suggest that Jahn–Teller (JT) distortion also plays a very important role in explaining the CMR effect [5,6]. Recently, some electronic and magnetic measurements have shown that the cation size mismatch at the La site in manganite perovskites affects magnetic properties and

[1] Corresponding author.

magnetoresistance. The ferromagnetic metal–paramagnetic insulator transition temperature decreases with a decrease in the average radius at the La site [7,8]. According to reports about the effects of the lattice on magnetoresistance, the tolerance factor is also a key parameter. Based on the above-mentioned experimental results and related theoretical models on the study of CMR materials, Millis [9] introduced an electron–lattice interaction model, which included the JT effect, the tolerance factor and the double exchange interaction, to explain the CMR effect in manganese perovskites. According to the double exchange mechanism, the ratio of Mn^{4+}/Mn^{3+} significantly affects the magnetic and electron transport properties of CMR materials and it is also possible to control the Mn^{4+}/Mn^{3+} ratio by element substitutions at Mn and O positions. More recently, the study of the effect of substitutions at the Mn position by 3d transition metals (such as Co, Fe and Cr) has been a topic of active research [10, 11]. However, reports studying the replacement of oxygen by other elements such as F and N are very limited. There are few reports on the effects of oxygen content and varying the oxygen isotope mass content in ABO_3 type perovskites [12,13]. In our previous work we have studied the structure, magnetic properties and CMR of the fluoride $R_{2/3}A_{1/3}MnO_{3-2x}F_{2x}$(R = La, Nd; A = Ca, Sr) [14]. An MR ratio as high as 99.2% was obtained in an F-doped (Nd, Sr)MnO_3 compound with an applied magnetic field of 5 T. In the present paper, a nitrogenated $La_{2/3}Ca_{1/3}MnO_3$ compound has been synthesized, and its structural, magnetic and electron transport properties have been investigated systematically. This experiment was designed in accordance with the nitrogenation method used in the intermetallics. We mention here that although the nitride process is fully developed for use in the synthesis of the rare earth–3d transition metal–metal (R–T–M) permanent magnetic materials with a Th_2Zn_{17}, Th_2Ni_{17} or $ThMn_{12}$ structure, this method has not been used until now for polycrystalline CMR materials.

2. Experimental procedure

The sample of nitrogenated $La_{2/3}Ca_{1/3}MnO_3$ was synthesized by a solid state reaction under flowing nitrogen, both for calcination and sintering heat treatments. The starting materials La_2O_3, MnO_2 and $CaCO_3$ were mixed in stoichiometeric proportions and were calcined at 1373 K for 30 h. The first sintering procedure was done at 1473 K for 24 h. Then the powder was ground and pelletized and further sintering was carried out at 1473 K for 36 h. The sample was then allowed to cool to room temperature. The normal sample of $La_{2/3}Ca_{1/3}MnO_3$ was prepared under identical heating conditions without nitrogen gas flow. The x-ray diffraction (XRD) intensity data which were used for crystal structure analysis were collected by a Rigaku automatic diffractometer with a rotating anode and a 12 kW x-ray generator. Cu K_{α_1} radiation ($\lambda = 1.5406$ Å) and a graphic monochromator for diffracted beams were used. A step scanning mode was adopted with a scanning step of $0.02^\circ(2\theta)$. The positions of diffraction peaks were corrected by using high-purity Si as an internal standard. After normalization, the TREOR program [15] was used to index the XRD patterns. The diffraction data were analysed by using the Rietveld powder diffraction profile-fitting technique [16] to determine the crystal structural parameters. DIAMOND software [17] was employed to calculate the Mn–O bond lengths and Mn–O–Mn bond angles based on the structural refinement parameters. The thermomagnetic properties of these samples were determined by a commercial SQUID magnetometer in the temperature range from 5 to 400 K with an applied field of 1 kG. The temperature dependence of magnetoresistance was measured by means of a standard four-probe method at zero field and an applied field of 5 T.

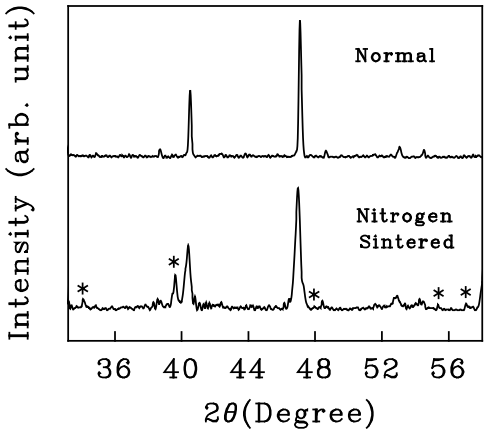

Figure 1. The XRD patterns of $La_{2/3}Ca_{1/3}MnO_3$ and its nitrogenated compound. The satellite peaks of the N superlattice are marked by asterisks.

Table 1. Indices of the satellite peaks: symmetry, orthorhombic; radiation, Cu K_{α_1} (1.540 56 Å), lattice parameters, $a = 3.541(2)$ Å, $b = 4.749(7)$ Å and $c = 7.873(7)$ Å.

h	k	l	d_{obs} (Å)	d_{cal} (Å)
0	1	2	3.021(4)	3.031(0)
1	0	2	2.625(6)	2.632(8)
0	2	1	2.271(8)	2.273(7)
2	0	0	1.771(7)	1.770(6)
2	1	0	1.660(4)	1.659(1)
2	0	2	1.612(2)	1.614(8)

3. Experimental results and discussion

The powder XRD pattern exhibits a single phase with an orthogonally distorted perovskite structure for the $La_{2/3}Ca_{1/3}MnO_3$ sample. The space group is *Pbnm*, with $Z = 4$. The lattice spacings are $a = 5.474(5)$ Å, $b = 5.459(5)$ Å and $c = 7.715(8)$ Å. In each unit cell, there are four equivalent crystal positions, i.e. $4a$, $4c(1)$, $4c(2)$ and $8d$ crystal position, which are occupied by 4Mn, 4(La,Ca), 4O I and 8O II respectively. However, there are a few weak satellite peaks observed to coexist with the orthorhombic phase in the XRD pattern for the nitrogenated sample as shown in figure 1. There are two possibilities for this phenomenon. One is due to an impurity phase, and the other is due to the superlattice. We have investigated all of the known possible binary and ternary oxides and nitrides (such as $CaMnO_3$, Ca_2MnO_4, La_2O_3, Mn_3O_4, Ca_3N_2) in the lanthanum–manganese–calcium–oxygen–nitrogen system as the possible impurity phase in this nitrogenated sample. However, we could not find a compound which fitted those satellite peaks. Although the low-angle XRD measurement is typically used to verify the supperlattice structure, we cannot perform this measurement due to limitations of the measurement range at our facility. According to the structural indexing results listed in table 1, we tentatively assign these satellite peaks to be a kind of superlattice due to N occupation in the lattice spacing with lattice parameters of $a = 3.541(2)$ Å, $b = 4.749(7)$ Å and $c = 7.873(7)$ Å. The figures of merit of these structural indices are $M = 70$ and $F = 22$ respectively. This kind of structure (orthorhombic phase and superlattice) has been refined by the Rietveld method. We have used several possible structural models for N occupation in

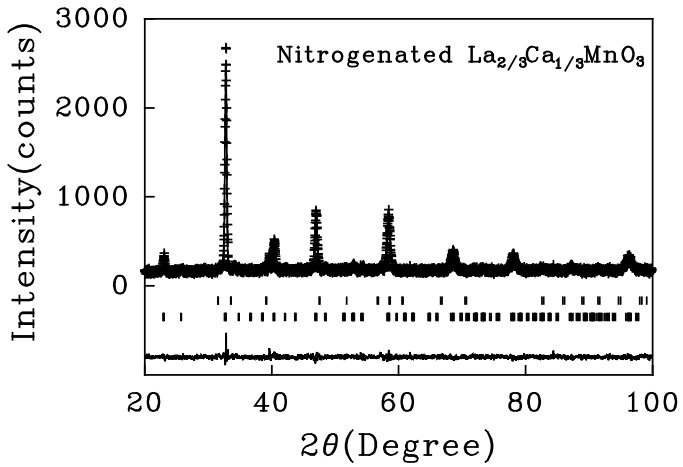

Figure 2. The refined XRD pattern of nitrogenated $La_{2/3}Ca_{1/3}MnO_3$.

Table 2. The structural refinement models for N atom occupation after nitrogenation of $La_{2/3}Ca_{1/3}MnO_3$.

N occupation	Satellite peaks fitting	$R_p(\%)$	$R_{wp}(\%)$	s
Substitution for O^{I} (4*c* 2)	No	6.0(7)	8.0(6)	1.1(4)
Substitution for O^{II} (8*d*)	No	6.1(1)	8.0(9)	1.1(5)
New 4*c* position	No	6.1(5)	8.1(4)	1.1(6)
New 8*d* position	No	6.1(9)	8.2(0)	1.1(8)
No N join	No	6.1(6)	8.1(7)	1.1(7)
	N superlattice + $La_{2/3}Ca_{1/3}MnO_3$			
4*c*	Yes	5.9(7)	7.6(0)	1.0(8)
8*d*	No	6.1(5)	8.1(5)	1.1(6)

the nitrogenated $La_{2/3}Ca_{1/3}MnO_3$ compound to fit these satellite peaks. The refined results are listed in table 2. According to the refined results, we suggest that the N atom joins the $La_{2/3}Ca_{1/3}MnO_3$ compound physically. It seems that the N atom does not substitute for O at the 4*c* and 8*d* sites nor does it occupy another 4*c* or 8*d* crystal position in the $La_{2/3}Ca_{1/3}MnO_3$ orthorhombic structure because these structural models cannot fit the extra satellite peaks. This implies that N should not been included in the $La_{2/3}Ca_{1/3}MnO_3$ formula index. However, if we consider that N occupation results in a superlattice structure, the satellite peaks can be fitted very well with a significant decrease of the weighted residual R factor. It seems that the superlattice model works for the nitrogenated $La_{2/3}Ca_{1/3}MnO_3$ compound. The refined XRD pattern for this superlattice structure model is shown in figure 2. The experimental and calculated patterns are marked by '+' and a full line respectively. The lowest trace indicates the difference between the two XRD patterns. The peak positions of the superlattice and orthorhombic structure are denoted by the vertical bars in the middle. The residual factor is $R_p = 5.9(7)\%$, and the weighted residual factor is $R_{wp} = 7.6(0)\%$, with a good fit factor of $s = 1.0(8)$, which confirms that the refinement is acceptable. Based on the structural refinement, the lattice parameters of the orthorhombic structure increase due to the formation of the superlattice, and the nitrogenation results in a increase of 0.88% in the unit cell volume. In the superlattice structure, the space group is *Pbnm*, with $Z = 4$, and the N atom prefers

Table 3. The refined structural parameters, coordination of Mn and ionic occupations, the distortion of MnO_6 octahedra and tolerance factor of $La_{2/3}Ca_{1/3}MnO_3$ (*Pbnm*, $Z = 4$) before and after nitrogenation.

	Normal sample	Nitrogenated sample
a (Å)	5.474(5)	5.495(1)
b (Å)	5.459(5)	5.472(1)
c (Å)	7.715(8)	7.736(7)
v (Å^3)	230.6(1)	232.6(4)
	Ionic occupations	
R(La,Ca)	x, 0.4860(5)	0.4863(4)
$4c(x, y, 1/4)$	y, 0.0223(4)	0.0225(8)
	Mn:4a(0,0,0)	
O I	x, 0.5326(7)	0.5345(9)
$4c(x, y, 1/4)$	y, 0.4984(1)	0.4948(1)
O II	x, 0.2031(3)	0.2176(8)
$8d(x, y, z)$	y, 0.2807(7)	0.3001(5)
	z,0.0146(4)	0.0159(5)
R_p	5.9(4)%	5.9(7)%
R_{wp}	7.4(9)%	7.6(0)%
s	1.19	1.08
	MnO_6 octahedron distortion	
Ion–ion	BL (Å) NN	BL (Å) NN
Mn– O I	1.937, 2	1.944, 2
Mn–O II	1.897, 2	1.902, 2
Mn– O II	2.022, 2	2.036, 2
⟨Mn–O⟩	1.952, 6	1.961, 6
Mn– O I–Mn(°)	169.39, 2	168.65, 2
Mn– O I–Mn(°)	161.14, 4	159.92, 4
⟨O–Mn–O⟩(°)	163.89, 6	162.83, 6
Tolerance factor	0.923	0.914
	Superlattice structure	
lattice: $a = 3.541(2)$ Å, $b = 4.749(7)$ Å, $c = 7.873(7)$ Å		
Occupation: N 4c (0.6348(8), 0.0205(8), 1/4)		
N–N: 2.511 Å		

to occupy the 4c crystal position. Table 3 shows the refined structural parameters, ionic occupations, the calculated nearest Mn–O bond lengths and neighbours of Mn and Mn–O–Mn bond angles for $La_{2/3}Ca_{1/3}MnO_3$ before and after nitrogenation.

Although both $La_{2/3}Ca_{1/3}MnO_3$ and the N superlattice have the same space group of *Pbnm*, the two structures cannot be shown in one structural frame due to their different lattice parameters. So, in order to show the two structures in one structural frame, the occupation parameters of the N lattices have been recalculated using the formula $X_i = (A_i/a_i)x_i$ ($i = 1, 2, 3$), where A_i and a_i denote the lattice parameters of the orthorhombic phase and N superlattice respectively; X_i and x_i correspond to the occupation parameters of N in the orthorhombic structure and the N superlattice respectively. After having changed these occupation parameters, the distributions and orientations of the MnO_6 octahedra and (La, Ca) lattices as well as the N lattices are shown by their projections on planes perpendicular to the

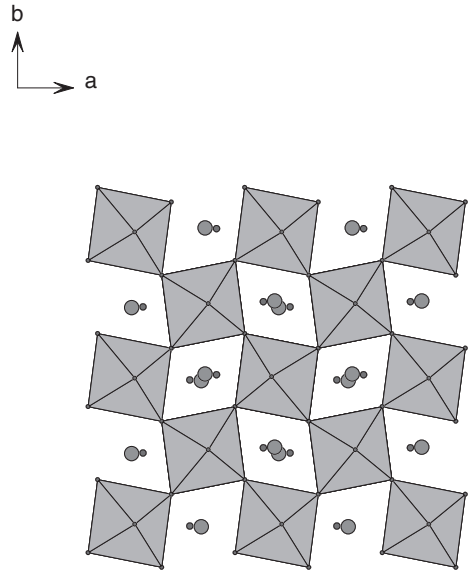

Figure 3. The projection perpendicular to the *c*-axis of the structures of the nitrogenated compound, where the (La, Ca) and N lattices are denoted by large filled circles and small filled circles respectively. The dots at at the corners of octahedra denote the O anions and the Mn cation is at the centre of the octahedron.

c-axes as illustrated in figure 3. The four N atoms are distributed between O I (which is at the top corner of the MnO_6 octahedron) and (La, Ca) lattices.

The correlation between the structural and physical properties, such as magnetic and electron transport properties and magnetoresistance, for nitrogenated $La_{2/3}Ca_{1/3}MnO_3$ has been investigated in this paper. The stoichiometric perovskite ABO_3 is cubic, but most alkaline-earth doped $RMnO_3$ compounds crystallize in the distorted orthorhombic, rhombic or tetragonal structure. One possible origin for the lattice distortion is the deformation of the MnO_6 octahedron arising from the JT effect, which is inherent in the high-spin ($S = 2$) Mn^{3+} with a doubly degenerate e_g orbital. Another possible source of distortion may be from the connection pattern of the MnO_6 octahedron in the perovskite structure, forming an orthorhombic lattice. In this case, the MnO_6 octahedron shows alternative buckling. Such a lattice distortion of the perovskite in the form ABO_3 is governed by the tolerance factor. The important aspect of the JT effect in the present case has been investigated by studying the distortions of MnO_6 octahedra based on the refined structural parameters, which include the Mn–O bond lengths and Mn–O–Mn bond angles. The tolerance factor has been calculated according to the equation

$$t = \frac{\langle d_{A-O} \rangle}{\sqrt{2}\langle d_{Mn-O} \rangle} \tag{1}$$

where $\langle d_{A-O} \rangle$ and $\langle d_{Mn-O} \rangle$ denote the average (La, Ca)–O and Mn–O bond lengths respectively. The calculated results are listed in table 3. Based on the calculated results, the distortion of the MnO_6 octahedron after nitrogenation shows an increase along the three Mn–O bond lengths and a decrease in the related Mn–O–Mn bond angles. The R–O (R: La, Ca) bond length tends to decrease, which results in a decrease in the tolerance factor. Such an MnO_6 octahedral distortion is described as a buckling. The effective Mn–Mn electron hopping is a very sensitive function of this buckling and decreases rapidly as the buckling increases. This structural

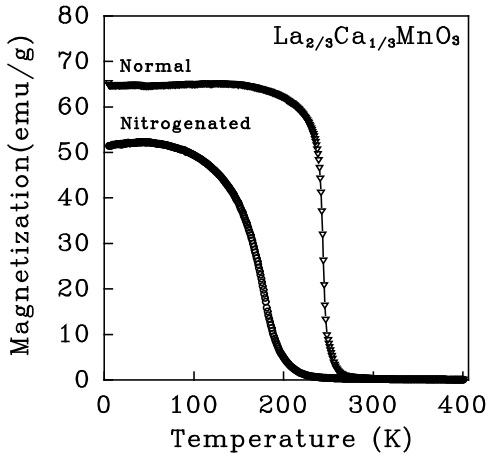

Figure 4. The temperature dependence of magnetization of $La_{2/3}Ca_{1/3}MnO_3$ before and after nitrogenation.

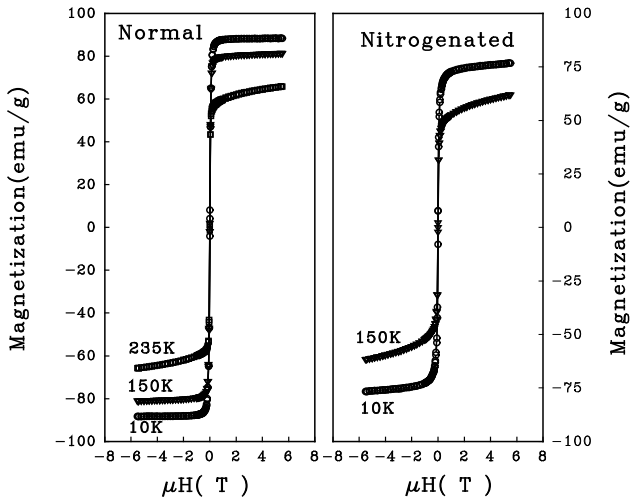

Figure 5. The applied magnetic field dependence of magnetization of $La_{2/3}Ca_{1/3}MnO_3$ before and after nitrogenation.

distortion most likely induces the decrease of T_C and MI transition temperatures, which is evident from our experimental results of the magnetic and electron transport properties.

Both $La_{2/3}Ca_{1/3}MnO_3$ and its nitrogenated compound exhibit the ferromagnetic ordering shown in figure 4, but the nitrogenation results in a 62 K decrease in the Curie temperature. This probably occurs due to the increase in the lattice parameters. Figure 5 shows the magnetic field dependence of magnetization for the normal sample and its nitrogenated compound. The saturation magnetic moments (M_s), which are obtained from the magnetic isotherms by extrapolating the $M(1/B)$ curves to $1/B = 0$ [18], are 3.31 and 2.94 μ_B/Mn for the $La_{2/3}Ca_{1/3}MnO_3$ before and after nitrogenation. The P_{eff} found by the Curie–Weiss law in the paramagnetic region corresponds to 5.16 μ_B for the normal compound and 5.23 μ_B for the nitrogenated compound.

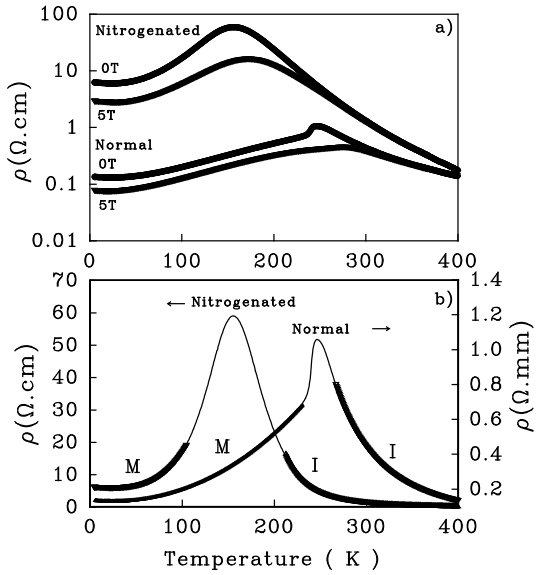

Figure 6. (*a*) The magnetoresistance versus temperature measured at zero field and an applied field of 5 T. (*b*) The resistivity fits for the two compounds, where M and I denote the fits in the metal and insulator regimes.

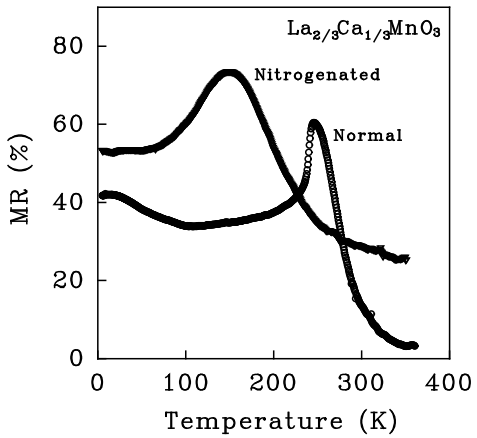

Figure 7. The temperature dependence of the magnetoresistance ratio of $La_{2/3}Ca_{1/3}MnO_3$ before and after nitrogenation.

The temperature dependence of the electrical resistivity ρ for $La_{2/3}Ca_{1/3}MnO_3$ and its nitrogenated sample is presented in figure 6(*a*) at applied fields of zero and 5 T. We observe that the nitrogenation increases the resistivity by more than one order of magnitude. The MR ratio increases by 15% from 63 to 78% after the nitrogenation, as shown in figure 7. We also notice a substantial decrease in the MI transition temperature from 246.6 K in $La_{2/3}Ca_{1/3}MnO_3$ to 156.3 K in the nitrogenated compound. In comparison with the decrease in the T_C value (62 K) induced by nitrogenation, the decrease in the MI transition temperature (90.3 K) is much greater. The possible reason for the difference in the shifts of T_C and MI transition temperature due to N incorporation might be explained as follows: the N atoms sits between

the lattice spaces thereby causing the Mn–O bond length to increase. As a result the double exchange interaction between Mn^{3+} and Mn^{4+} is reduced due to the presence of an N atom between them. Hence there is a reduction in T_C value. Thus the only purpose of the N atom in the magnetization is to reduce the Mn–Mn interaction. However, considering resisitivity, N atoms can act as a potential source of scattering and therefore the overall resisitivity will increase. Also the N atoms most probably play a role in charge trapping (or localization) along with the usual JT distortions present in the lattice. This can always happen because the N atom introduces a distortion in the lattice and can also act as a source of distortion itself. Thus the combined effect is that localization takes place due to JT distortion as well as N-induced distortions. Hence the reduction in the MI transition temperature is more pronounced. The low-temperature zero-field resistivity exhibits a shallow minimum at 23.9 and 23.8 K for the normal and nitrogenated compounds respectively. This low-temperature minimum decreases with the application of a magnetic field.

In the ferromagnetic region the electrical resistivity data for the two compounds at an applied magnetic field of $H = 0$ and 5 T fits the following expression very well:

$$\rho = \rho_0(1 - aT + bT^2 + cT^4) \tag{2}$$

where ρ_0 is the temperature-independent residual resistivity. The $\rho_0 bT^2$ term is most probably due to electron–spin scattering in the ferromagnetic phase. The $\rho_0 cT^4$ term gives a good fit to the experimental data and is probably due to electron–phonon scattering. However, one must note that the coefficient c is very small. The negative term $-\rho_0 aT$ in equation (2) is related to a grain boundary effect discussed below. The fit to our experimental data is further supported by a similar fit to resistivity data for thin film of $La_{2/3}Ba_{1/3}MnO_3$ in the temperature range up to 150 K found by Lofland *et al* [19]. However, Lofland *et al* do not provide the reason for the negative term in equation (2). Zhao *et al* [20] have explained the low-temperature resistivity of epitaxial thin films of $La_{1-x}Ca_xMnO_3$ using a theory of small polaron metallic conduction. However, this theory does not explain the negative term in polycrystalline sample resistivity at low temperature either and the fit is good only below 80 K, i.e. in the range of $T \ll T_C$. The resistivity data in our case fit to equation (2) very well until very close to T_C. The low-temperature minimum in resistivity data and the $-\rho_0 aT$ term in equation (2) is probably caused by charge carriers tunnelling between antiferromagnetically coupled grains [21]. Recently, Rozenberg *et al* [21] have provided a model explaining the observation of a resistance minimum in the (La, Pb)MnO_3 system.

In our case, the resistivity fits equation (2) very well for experimental measurements in the temperature range of more than half of the T_C. The fitting parameters of the normal compound and its nitrogenated compound are listed in table 4. All of these fitting parameters decrease with applied magnetic field, especially for the ρ_0 and $a\rho_0$ term. This shows that the applied field suppresses the temperature-independent resistivity, the grain boundary effect and all of the scattering interactions. The enhancement of the resistivity due to nitrogenation is probably due to two contributions that come from the structural distortion of the orthorhombic phase and the nitrogen superlattice. In the insulating regime, the resistivity follows the equation $\rho = \rho_0 \exp(E/k_B T)$, where the E/k_B values correspond to 1420.9 and 1792.1 K for $La_{2/3}Ca_{1/3}MnO_3$ and its nitrogenated compound at zero field. The fit to the data are given in figure 6(*b*). Separately in figures 8(*a*) and (*b*) we show the fit to the experimental data in the metallic region.

4. Conclusion

In conclusion, nitrogenation of $La_{2/3}Ca_{1/3}MnO_3$ increases the lattice parameters and unit cell volume, and induces the formation of a superlattice structure. The N atom prefers to occupy

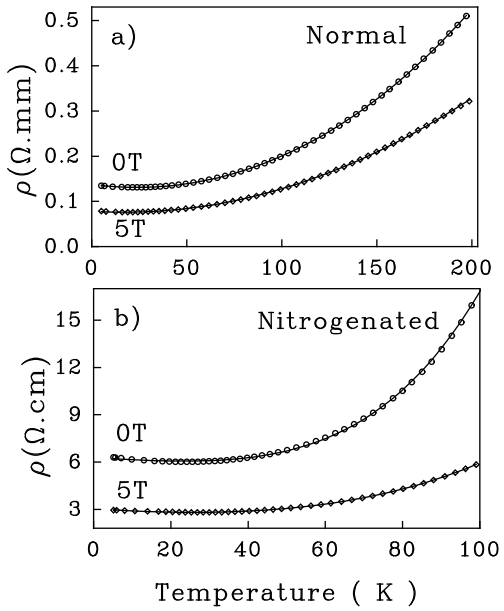

Figure 8. (*a*) The metal resistivity fitting curves of the normal $La_{2/3}Ca_{1/3}MnO_3$ and (*b*) its nitrogenated compound at zero field and an applied field of 5 T, where the experiment and resistivity fits are denoted by the symbols and full curve respectively.

Table 4. The resisitivity fitting paremeters for $La_{2/3}Ca_{1/3}MnO_3$ before and after nitrogenation.

	ρ_0(mΩ cm)	$a(10^{-3}$ K$^{-1})$	$b(10^{-5}$ K$^{-2})$	$c(10^{-10}$ K$^{-4})$
Normal sample at 0 T	13.7(7)	4.02(1)	8.42(4)	1.55(4)
Nitrogenated sample at 0 T	6311.(9)	3.03(8)	4.92(1)	147.(3)
Normal sample at 5 T	7.8(7)	3.38(2)	9.65(6)	0.009(5)
Nitrogenated sample at 5 T	3054.(4)	5.97(5)	10.9(5)	44.6(6)
		$a\rho_0(\mu\Omega$ cm K$^{-1})$	$b\rho_0(\mu\Omega$ cm K$^{-2})$	$c\rho_0$(pΩ cm K^{-4})
Normal sample at 0 T		55.3(7)	1.16(2)	2.14(4)
Nitrogenated sample at 0 T		19 180.(3)	310.(6)	92 950.(1)
Normal sample at 5 T		26.6(2)	0.7(6)	0.007(5)
Nitrogenated sample at 5 T		18 250.(2)	344.(4)	13 640.(1)

the 4*c* crystal position. The nitrogenation results in a decrease in the Curie temperature and the average magnetic moments. The effect of nitrogenation on the electron transport properties is to give a very large increase in the resistivity. However, the resistivity still exhibits an MI transition even though the MI transition temperature decreases. The resistivity behaviour follows the relation $\rho = \rho_0(1 - aT + bT^2 + cT^4)$ in the metal regime and $\rho = \rho_0 \exp(E/k_B T)$ in the insulator regime. Based on the relationship between structural and physical properties, we suggest that the distortion of the MnO_6 octahedron with the consequent increase in Mn–O bond lengths and decrease of Mn–O–Mn bond angles as well as the decrease of the tolerance factor result in the reduction of T_C and the MI transition temperature after nitrogenation.

Acknowledgment

This work was supported by a grant from the Consortium for Advanced Radiation Source, University of Chicago.

References

[1] von Helmolt R, Wecker J, Holzapfel B, Schultz L and Samwer K 1993 *Phys. Rev. Lett.* **71** 2331
[2] Jin S, Tiefel T H, McCormack M, Fastnacht P A, Ramesh R and Chen L H 1994 *Science* **264** 413
[3] Briceno G 1995 *Science* **270** 273
[4] Zener C 1951 *Phys. Rev.* **82** 403
[5] Millis A J, Littlewood P B and Shraiman B I 1995 *Phys. Rev. Lett.* **74** 5144
[6] Coey J M D, Viret M, Ranno L and Ounadjeda K 1995 *Phys. Rev. Lett.* **75** 3910
[7] Hwang H Y, Cheong S-W, Radaelli P G, Marezio M and Batlogg B 1995 *Phys. Rev. Lett.* **75** 914
[8] Sundaresan A, Maignan A and Raveau B 1997 *Phys. Rev.* B **56** 5092
[9] Millis A J 1998 *Nature* **392** 147
[10] Briceno G, Chang H Y, Sun X D, Schultz P G and Xiang X D 1995 *Science* **270** 273
[11] Perez J, Garca J, Basco J and Stankiewicz J 1998 *Phys. Rev. Lett.* **80** 2401
[12] Zhao G M, Conder K, Kerller H and Müller K A 1996 *Nature* **381** 676
[13] Ju H L, Gopalakrishnan J, Peng J L, Li Q, Xiong G C, Venkatesan T and Greene R L 1995 *Phys. Rev.* B **51** 6143
[14] Guo Y Q *et al* 1999 *J. Solid State Chem.* **148** 236
Guo Y Q *et al* 2000 *J. Alloys Compd.* **296** 33
Guo Y Q *et al* 2000 *J. Alloys Compd.* **306** 133
[15] Werner P E 1965 *J. Appl. Crystallogr.* **9** 594
[16] Rietveld H M 1969 *J. Appl. Crystallogr.* **2** 65
[17] Werber S 1999 *J. Appl. Crystallogr.* **32** 1028
[18] Dionne G F 1969 *J. Appl. Phys.* **40** 1839
[19] Lofland S E *et al* 1995 *Phys. Rev.* B **52** 15 058
[20] Zhao G M *et al* 2000 *Phys. Rev. Lett.* **84** 6086
[21] Rozenberg E *et al* 2000 *J. Appl. Phys.* **88** 2578